Structure and dynamics of the summertime atmospheric boundary layer over the Antarctic Plateau: 1. Measurements and model validation

Dirk van As,[1] Michiel R. van den Broeke,[1] and Michiel M. Helsen[1]

Received 5 March 2005; revised 17 June 2005; accepted 23 August 2005; published 4 April 2006.

[1] Profile mast, tethersonde and radiosonde measurements are used to describe the structure and dynamics of the summertime atmospheric boundary layer over the slightly sloping snow surface at Kohnen base (75°00′S, 0°04′E, 2892 m above sea level), located on the interior plateau of East Antarctica. During a 4-day clear-sky period at the end of summer, we found a shallow but dynamic boundary layer. Net radiation contributed between −40 and +35 W m^{-2} to the surface energy balance and was negative on average; the sensible and latent heat fluxes contributed less than 10 W m^{-2} and 1 W m^{-2}, respectively; the subsurface heat flux mostly counteracted the radiative flux. Owing to nighttime radiative cooling at the surface an increasingly deep stable layer formed with a temperature deficit of over 12 K. Within this layer we observed a katabatically driven low-level jet which increased in altitude from 20 to 70 m during the night and persisted up to noon. By that time a shallow mixed layer was deepening and warming underneath the stable layer. The mixed layer obtained a maximum depth of 70 m halfway through the afternoon. During the experiment the ABL was near saturation. The observations were used to validate a one-dimensional atmospheric boundary layer model.

Citation: van As, D., M. R. van den Broeke, and M. M. Helsen (2006), Structure and dynamics of the summertime atmospheric boundary layer over the Antarctic Plateau: 1. Measurements and model validation, *J. Geophys. Res.*, *111*, D07102, doi:10.1029/2005JD005948.

1. Introduction

[2] The Antarctic ice sheet has an important role in the global atmospheric circulation due to its position, shape and the radiative and insulating properties of its snow-covered surface. The interaction between the ice sheet and the atmosphere largely takes place in the atmospheric boundary layer (ABL). Because of the highly reflective Antarctic snow surface, even in mid-summer absorption of solar radiation is low, causing only weak buoyancy-driven turbulence and therefore a shallow ABL of at most a few hundred meters deep. More characteristic over Antarctica is the stable ABL. This surface-based temperature inversion forms at night and during winter due to a negative surface radiation budget. A low-level jet occurs in the stable ABL when the relatively cold and dense layer of air is gravitationally forced down a sloping surface, i.e., katabatic wind [*Ball*, 1956].

[3] Most observational studies of the Antarctic ABL were performed at low elevations. *Heinemann* [1988] discussed the heat budget of the ABL at the ice front of the Ronne Ice Shelf using profile measurements of a summertime experiment in 1983/1984 and found a dominant contribution of horizontal advection. *King* [1989] used ABL observations to show that for the coastal base Halley low-level winds are often katabatically dominated, explaining their high directional constancy. Only for strong large-scale forcing opposing the katabatic forcing, near-surface winds are reversed. *Kottmeier* [1986] showed that for the flow in the stable ABL over the Ekström Ice Shelf, katabatic forcing does not dominate the momentum budget.

[4] *Sorbjan et al.* [1986] presented profiles of ABL temperature and wind speed in the escarpment region of Adélie Land in the summer of 1982/1983. They found no significant daily cycle in near-surface wind direction and contributed it to the alignment of katabatic and geostrophic forcings. *Kodama et al.* [1989] observed ABL wind speed maxima during both day and night for the same location. They found that at night the jet was katabatically forced, but during the day the shear in wind speed was caused by a mesoscale horizontal temperature gradient which is due to the temperature contrast between the ocean and Antarctic interior. *Bintanja* [2000] concluded from an ABL experiment at the inland station Svea (located in the escarpment region of Dronning Maud Land (DML) (Figure 1)) that the influences of geostrophic and thermal winds on the summertime ABL decrease toward the Antarctic interior and that katabatic forcing dominates the near-surface wind field, especially during clear-sky conditions.

[5] This paper presents the observed structure and dynamics of the ABL during the EPICA-Netherlands Atmospheric Boundary Layer Experiment (ENABLE), which was performed at Kohnen base (75°00′S, 0°04′E, 2892 m above

[1]Institute for Marine and Atmospheric Research Utrecht, Utrecht University, Utrecht, Netherlands.

0148-0227/06/2005JD005948$09.00

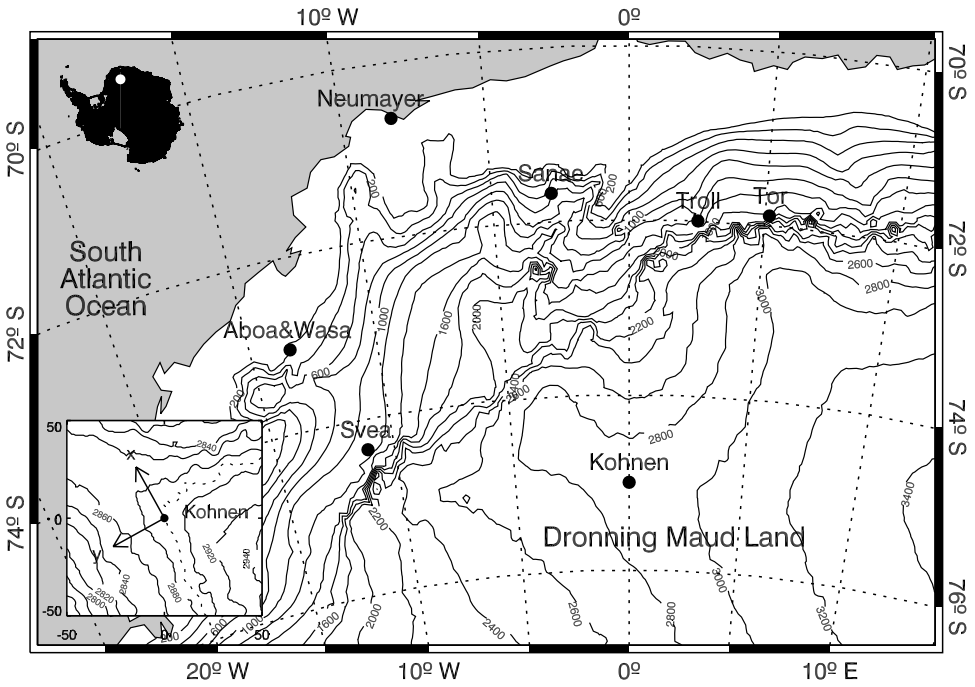

Figure 1. Elevation map of Dronning Maud Land with inset maps of Antarctica and Kohnen surroundings. Elevation data are derived from the 1 × 1 km Radarsat Antarctic Mapping Project digital elevation model version 2. The x and y vectors point in the local cross-slope and down-slope direction, respectively.

sea level) (Figure 1) in DML on the high Antarctic Plateau. The campaign took place between 7 January and 11 February 2002, at the end of the Antarctic summer. In this period the relatively large diurnal insolation amplitude forces a strong daily cycle within the ABL [*van As et al.*, 2005b].

[6] Few observational studies of the ABL have been performed on the Antarctic Plateau. Observations of the ABL structure have been presented for Dome C and South Pole [e.g., *Mastrantonio et al.*, 1999; *Mahesh et al.*, 1997]. These bases have approximately the same surface elevation as Kohnen (3233 m and 2841 m above sea level, respectively), but comparison is hampered by crucial factors such as the time of year during the experiment, the surface slope (no katabatic forcing at Dome C) and latitude (no daily cycle in shortwave radiation at South Pole). *Mastrantonio et al.* [1999] showed that for the same insolation, temperatures and wind speeds as observed during ENABLE, convection occurs and a mixed layer develops during clear-sky days. Daytime sensible heat fluxes are slightly larger than at Kohnen (-20 W m^{-2} for the end of January). A convective ABL of 150 m depth was observed at Dome C. *Mahesh et al.* [1997] devised a correction method for response-time related temperature measurement errors by radiosondes in strong near-surface temperature inversions at South Pole station.

[7] This paper discusses the structure and dynamics of the summertime ABL over the Antarctic interior using high-resolution balloon and mast observations, and with this fulfills the main objective of the ENABLE campaign. We also use the observations to validate a one-dimensional ABL model with high near-surface resolution. In a companion paper results of this model simulation will be used to assist in the quantitative interpretation of the observations [*van As and van den Broeke*, 2006]. The model validation in this paper enables us to apply the model to other Antarctic sites, which will be done in a forthcoming paper. Model-based studies of the Antarctic ABL were also performed by, for example, *Brost and Wyngaard* [1978], *King* [1989], *van den Broeke et al.* [2002], *Parish and Cassano* [2003] and *Renfrew* [2004].

[8] This paper is organized as follows: the surroundings of Kohnen base and the prevailing meteorological conditions are described in section 2. The measurements and model are discussed in section 3. The measured daily cycle of the boundary layer are presented and compared to model results in section 4. Hereafter a discussion follows in section 5 and the findings are summarized in section 6.

2. Location and Meteorological Conditions

[9] Kohnen base is located on the high plateau of East Antarctica (see Figure 1), approximately 550 km from the South Atlantic coastline and 200 km from the escarpment region. This location is typical for a large part of the Antarctic Plateau in the sense that it is positioned away from the pole (which results in a daily cycle in shortwave radiation (SR) in summer) and has a small but significant surface slope. It is set apart from most interior locations as the mean easterly large-scale wind is almost aligned with the surface slope instead of being more typically cross-slope oriented [*van den Broeke et al.*, 2002]. The snow surface slopes upward by 1.3 ± 0.3 m km^{-1} toward the east-northeast (61 ± 15°), as derived from the 1 × 1 km Radarsat Antarctic Mapping Project digital elevation model version 2

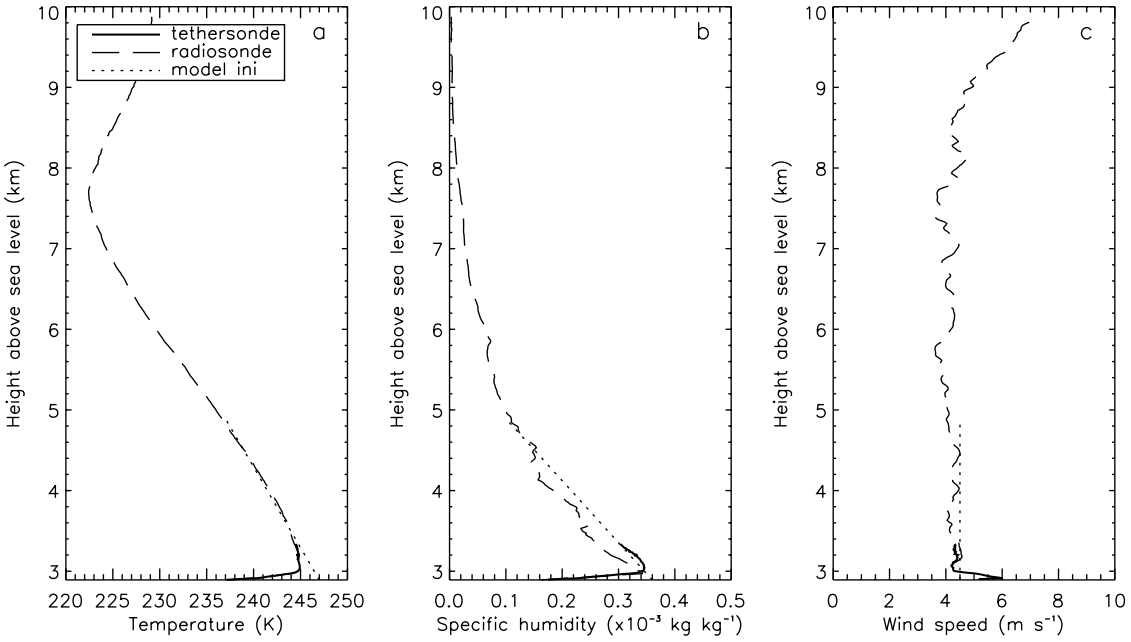

Figure 2. Four-day mean profiles of (a) temperature, (b) specific humidity, and (c) wind speed, determined by tethersonde (solid lines) and radiosonde measurements (dashed lines) during ENABLE. On the basis of these measurements, profiles were chosen for model initialization (dotted lines).

[*Liu et al.*, 2001]. Figure 1 shows that Kohnen is located on a topographic ridge.

[10] Automatic weather station measurements since December 1997 indicate that 2 m temperatures (T) near Kohnen range from daily mean values of approximately 215 K in mid-winter to 250 K in mid-summer. On a few occasions wintertime temperatures have dropped to as low as 202 K. Low temperatures in the Antarctic interior are caused by a combination of factors: high latitude, high elevation, high surface albedo and consequently a strongly negative radiation budget which forces a strong surface-based temperature inversion. Low temperatures invoke low specific humidities (q), which range from typically 0.5 g kg^{-1} in summer to less than 0.1 g kg^{-1} in winter at Kohnen. Wind speed (U) and direction (d) at 2 m height do not show a significant seasonal cycle and have mean values of 4.8 m s^{-1} and 57°, respectively.

[11] The flow of cold and dry air in approximate downslope direction in the ABL is interrupted several times per year by synoptic-scale disturbances. These events transport relatively warm and moist air originating from the South Atlantic Ocean and are often accompanied by snowfall. In winter, near-surface temperatures can rise by tens of degrees, and 2 m wind speeds can increase up to 20 m s^{-1} during these events.

[12] In the ENABLE measurement period one such strong-wind event occurred, after which the atmosphere was cooling strongly, with daily mean temperatures at 2 m height falling from 259 K to 236 K. The average profiles of T, q and U during the clear-sky period that is the focus of this paper (31 January to 3 February) are shown in Figure 2. The tropopause is located at almost 8 km above the sea surface. The temperature lapse rate in the troposphere is -6×10^{-3} K m^{-1}. Specific humidity (q) decreases with altitude and U is fairly constant (3.5–4.5 m s^{-1}) in the troposphere.

3. Methods

3.1. Measurements

[13] Profile mast (PM) measurements of temperature, relative humidity (RH) and wind speed were performed every 2 min at heights of 0.5, 1, 2, 5 and 10 m above the surface. T and RH were measured with ventilated Vaisala HMP35C sensors and wind speed with Vector A100R cup anemometers. Wind direction measurements were performed at 2 and 10 m using Vector wind vanes. For sensor accuracy see Table 1.

[14] Twice per day, at approximately 1100 and 2300 GMT, Vaisala RS-90 AG radiosondes (RS) with GPS wind-finding were released, reaching altitudes of typically 20 km above sea level. An average (nearly constant) ascent rate of 2.8 m s^{-1} and a sample frequency of 1 Hz implies one measurement every 2.8 m on average.

[15] A helium-filled tethered balloon, equipped with an AIR TS-5A-SP sonde, was used 8 times per day to obtain

Table 1. Measurement Accuracies of Pressure, Temperature, Relative Humidity, Wind Speed, and Wind Direction by Profile Mast, Tethersonde, and Radiosondes as Obtained From Sensor Manuals

Parameter	Profile Mast	Tethersonde	Radiosondes
p	not measured	1 hPa	1.5 hPa[a]
T	0.2 K	0.5 K	0.5 K[a]
RH	2% (RH < 90%) 3% (RH > 90%)	3%	5%[a]
U	0.1 m s^{-1}	0.5 m s^{-1}	0.5 m s^{-1}
d	2°	10°	unknown

[a]Cumulative uncertainty including repeatability, effects due to measuring conditions, and response time.

vertical profiles of T, RH, U and d up to an average height of 500 m above ground level. As opposed to RS measurements, which are not restricted to fine weather, the tethersonde (TS) system could only be deployed for wind speeds smaller than 15 m s^{-1}. In total, 89 TS profiles were obtained, covering eleven days. Ascent and descent rates in the ABL were kept low to obtain two to four measurements per meter at a sampling rate of 0.5 Hz.

[16] All three measurement systems mentioned above measure RH relative to water instead of ice, which results in significant errors at low temperatures. RH measurements were corrected according to the method proposed by *Anderson* [1994], who showed that the procedure is suitable for coastal station Halley [*Anderson*, 1996]. As the correction procedure is increasingly accurate for an increasing number of RH measurements (in particular at near saturation), the profile mast humidity measurements are most reliable. Owing to the small amount of measurements at near saturation, TS and RS measurement accuracies of RH are likely to be lower than the accuracies from the sensor manuals (Table 1). Specific humidity is calculated from RH measurements using the saturation vapor pressure equation of *Curry and Webster* [1999].

[17] Incoming and outgoing shortwave and longwave radiation (LR) fluxes were measured with a Kipp and Zonen CNR1 sensor. This type of sensor produces unreliable incoming shortwave radiation (SR_{in}) measurements for radiation originating from large zenith angles (>80°). These measurements were corrected according to the method proposed by *van den Broeke et al.* [2004].

[18] Sensible and latent heat fluxes (H_S and H_L) were calculated from 2 m PM measurements using the one-level bulk method in accordance with the Monin-Obukhov similarity theory. For this we used a constant surface roughness length for momentum (z_0) of 2×10^{-5} m as determined from sonic anemometer measurements; the roughness lengths for heat and humidity (z_T and z_q) were calculated using the method by *Andreas* [1987], which resulted in values of z_0, z_T and z_q of the same order of magnitude. The stability-correction functions by *Holtslag and de Bruin* [1988] and *Dyer* [1974] were used for stable and unstable stratifications, respectively. Surface temperature was calculated from outgoing longwave radiation (LR_{out}), assuming the snow surface to have unit emissivity in the longwave part of the spectrum. Surface specific humidity was calculated from temperature assuming saturation at the surface. These calculated turbulent fluxes compare well with direct turbulent flux measurements using eddy correlation techniques [*van As et al.*, 2005a].

[19] The subsurface heat flux (G) was calculated using the effective thermal conductivity equation by *Östin and Andersson* [1991]. An initial snow temperature profile was obtained from thermistor string measurements at the beginning of ENABLE. All subsequent T profiles were allowed to change by energy exchange at the surface and thermal diffusion within the snow layer. Calculated snow temperatures compare well to measured snow temperatures, which implies a good accuracy of G at the surface.

[20] For a detailed discussion of the measurements within the SL and calculation of the SEB components during ENABLE we refer to *van As et al.* [2005a, 2005b].

3.2. Model

[21] A one-dimensional ABL model was used to simulate the observations during ENABLE. The code was originally developed by *Duynkerke* [1991] to simulate radiation fog. A subsurface heat flux parameterization for a homogeneous slab soil is included [*Deardorff*, 1978]. Clear-sky downwelling longwave radiation uses the parameterization of *Rodgers* [1967], which takes into account the effects of water vapor, liquid water and carbon dioxide. The shortwave radiation parameterization includes scattering and absorption by clouds and atmospheric gasses [*Fouquart and Bonnel*, 1980]. *Duynkerke* [1991] showed that the model performs well for moderately stable conditions encountered at midlatitudes during clear skies at night.

[22] The model has been adapted for clear-sky Antarctic conditions; it describes the ABL over a highly reflective and smooth sloping surface without vegetation or clouds. Saturation no longer leads to the formation of a liquid water fog, but is removed from the modeled atmosphere in the form of clear-sky precipitation (diamond dust) without interaction with radiation. Also the spatial and temporal resolution of the model has been increased. Two hundred vertical levels cover the lowest 2 km of the atmosphere with a nonlinear grid spacing increasing with altitude, ranging from 1.6×10^{-2} m to 18 m. The model time step is 5 min.

[23] The model solves the conservation equations of heat, moisture and momentum in a coordinate system with the x-axis aligned with the cross-slope direction and y-axis aligned with the fall-line. In this coordinate system, the approximate conservation equations are given by

$$\frac{\partial \theta}{\partial t} = -v\frac{\partial \theta}{\partial z}B_\theta \sin\beta - \frac{\partial \overline{w'\theta'}}{\partial z} - \frac{1}{\rho c_p}\frac{\partial R_{net}}{\partial z}, \tag{1}$$

$$\frac{\partial q}{\partial t} = -v\frac{\partial q}{\partial z}B_q \sin\beta - \frac{\partial \overline{w'q'}}{\partial z} - Q, \tag{2}$$

$$\frac{\partial u}{\partial t} = f\left(v - v_g\right) - \frac{\partial \overline{u'w'}}{\partial z}, \tag{3}$$

$$\frac{\partial v}{\partial t} = -f\left(u - u_g\right)\cos\beta - \frac{\partial \overline{v'w'}}{\partial z} - g\frac{\theta - \theta_0}{\theta_0}\sin\beta, \tag{4}$$

where

$$B_{\theta/q} = \frac{\sin\beta - \sin\beta_{\theta/q}}{\sin\beta}, \tag{5}$$

where

θ	potential temperature;
$u/v/w$	wind speed in x/y/z direction;
u_g/v_g	geostrophic wind speed components;
t	time;
$\sin\beta$	surface slope;
$\sin\beta_{\theta/q}$	slope of isolines of θ/q in along-slope direction;
ρ	air density;
c_p	heat capacity of dry air (assumed constant at 1005 J K^{-1} kg^{-1});

R_{net} net radiation flux;
Q moisture sink due to precipitation;
f Coriolis parameter (-1.41×10^{-4} s^{-1});
g gravitational acceleration (9.81 m s^{-2});
θ_0 potential temperature extrapolated from the free atmosphere,

and primes indicate turbulent fluctuations. $B_{\theta/q}$ is a measure for the slope of the isolines of θ/q relative to the surface slope. For $B_{\theta/q} = 0$ the isolines are parallel to the surface and vertical advection has no contribution, for $B_{\theta/q} = 1$ the isolines are horizontal. The model incorporates turbulent mixing in accordance with local Monin-Obukhov similarity theory [*Nieuwstadt*, 1984], using stability-correction functions by *Duynkerke* [1991] and *Dyer* [1974] for stable and unstable stratification, respectively. The Duynkerke functions are approximately equal to the functions by *Holtslag and de Bruin* [1988] for a stability of $0 < z/L_* < 2$ (L_* is the Obukhov length scale), which were used to calculate the turbulent heat fluxes mentioned earlier. The turbulent fluxes in the model are calculated using

$$\overline{w'a'} = -K_{h/m}\frac{\partial a}{\partial z}, \tag{6}$$

where K_h is the turbulent diffusion coefficient for heat and moisture and K_m for momentum,

$$K_{h/m} = \frac{(\kappa z)^2}{\phi_m \phi_{h/m}}\left|\frac{\partial U}{\partial z}\right|, \tag{7}$$

where $\kappa = 0.4$ is Von Kármán's constant and $\phi_{h/m}$ are the stability-correction functions for heat and moisture/momentum.

[24] Energy exchange at the snow surface is governed by the surface energy balance (SEB). For a nonmelting, infinitely thin surface layer without heat capacity the SEB is

$$R_{net} + H_S + H_L + G = 0, \tag{8}$$

where

$$R_{net} = (1-\alpha)SR_{in} + LR_{in} + LR_{out}, \tag{9}$$

$$H_S = \rho c_p U_* T_*, \tag{10}$$

$$H_L = \rho L_s U_* q_*, \tag{11}$$

$$G = k_e \frac{T_0 - T_{-1}}{|z_0 - z_{-1}|}, \tag{12}$$

where

$$T_* = \frac{\kappa(T_1 - T_0)}{\ln(z_1 z_T^{-1}) - \psi_h}, \tag{13}$$

$$q_* = \frac{\kappa(q_1 - q_0)}{\ln\left(z_1 z_q^{-1}\right) - \psi_h}, \tag{14}$$

$$U_* = \frac{\kappa U_1}{\ln\left(z_1 z_0^{-1}\right) - \psi_m}, \tag{15}$$

Table 2. Constants and Initial Variable Values Used in Model Run

Parameter	Value
surface slope (sin β)	1.3 m km^{-1}
surface albedo (α)	0.85
surface pressure	670 hPa
T lapse rate (γ_T)	-5.0×10^{-3} K m^{-1}
extrapolated surface T	247 K
θ plane tilt parameter (B_θ)	0.5
q lapse rate (γ_q)	-0.13×10^{-6} m^{-1}
extrapolated surface q	0.36 g kg^{-1}
q plane tilt parameter (B_q)	0.3
geostrophic wind speed (U_g)	4.5 m s^{-1}
geostrophic wind direction	61° (down-slope)
soil/snow density	350 kg m^{-3}
initial snow T	240 K

where

α surface albedo;
T_* turbulent temperature scale;
q_* turbulent humidity scale;
U_* friction velocity;
L_s latent heat of sublimation (assumed constant at 2.83×10^6 J kg^{-1});
k_e effective thermal conductivity of snow (assumed constant at 0.274 W m^{-1} K^{-1});
T_i temperature at model level i (0 indicates surface);
q_i specific humidity at model level i;
U_i wind speed at model level i;
z_i vertical position of model level i;
$z_{T/q/0}$ surface roughness length for heat/moisture/momentum (all three assumed constant at 2×10^{-5} m);
$\psi_{h/m}$ $\int [1 - \phi_{h/m}]d\xi$.
ξ nondimensional stability parameter.

Positive surface fluxes transfer energy toward the surface.

[25] For the model simulations of the ABL at Kohnen base we selected a 4-day period between 31 January and 3 February 2002, which was a clear-sky and fair-weather period without strong large-scale atmospheric activity. We did not include clouds in the model as no TS observations have been performed during cloudy days and thus model results cannot be validated for overcast conditions. However, we have determined from AWS observations that low cloud amounts are common at Kohnen (cloud fractions below 40% occur an estimated 70% of the time). Table 2 lists model constants used [see also *van As et al.*, 2005a], as well as several initial values for variables. None of the parameters have been tuned to fit observations. Albedo is assumed constant at 0.85, which is approximately the mean daytime value of observed albedo during the simulated period. Initial values of temperature lapse rate, specific humidity, wind speed and direction were chosen on the basis of free-atmosphere measurements by TS and RS (Figure 2). Vertical advection of heat and moisture (first term on the right-hand side of equations (1) and (2), respectively) is partly dependent on the isoline-slant parameter B introduced above, which can not be determined from ENABLE observations. We estimated the parameter using monthly mean European Centre for Medium-range Weather Forecast re-analysis data (ERA-40) of temperature and specific humidity for January 2002. A sensitivity study will follow in a forthcoming paper, since model results can be

sensitive to, for example, geostrophic wind direction [*Brost and Wyngaard*, 1978].

[26] We have neglected large-scale subsidence, arising from the divergence in the katabatic wind field over Antarctica. Judging from ERA-40 data, heating and drying of the atmosphere due to large-scale subsidence over Kohnen is much smaller than the heating and drying due to vertical advection in the period of simulation. We estimate for instance the heating due to large-scale subsidence to be smaller than 0.4 K per day, arising from a vertical speed of -1 mm s^{-1}. This is a small heating rate compared to the temperature changes in the ABL which are up to 50 times larger, and will therefore not significantly influence the ABL structure and dynamics.

[27] By definition the ABL is the atmospheric layer which reacts to surface processes on timescales shorter than 1 day. Therefore the model was run one additional day prior to the period of simulation, in which the model created an initial boundary layer.

4. Results

4.1. Surface Energy Balance

[28] Figure 3 shows the SEB for the selected 4-day fair-weather period, preceded by one cloudy day. This day is included to highlight differences between the SEB of clear and cloudy skies and to demonstrate that one day is sufficient model spin-up time.

[29] SR_{in} observations vary between 25 and 670 W m^{-2}, absorbed SR peaks at 100 W m^{-2} (Figure 3a). Note that daytime SR_{net} is small compared to midlatitude clear-sky values (600–700 W m^{-2} [*Kottmeier*, 1986]) owing to high latitude and albedo. Observed LR_{in} contributes 120 W m^{-2}, showing a small daily cycle of 10 W m^{-2} (Figure 3b). LR_{out} follows surface temperature and oscillates by 40 W m^{-2}. LR_{net} values are negative; -40 W m^{-2} during the night and -80 W m^{-2} at noon. R_{net} is positive at daytime and negative at night, but negative on average (Figure 3c). Cloudy conditions (day 30) cause an overall positive radiation balance chiefly caused by a strong increase in LR_{in}, in spite of a 20% decrease in SR_{in} and a higher surface albedo for diffuse SR.

[30] The turbulent heat fluxes are also small (Figures 3d and 3e). H_L is very small (-1.2 to $+0.6$ W m^{-2}), owing to the low water vapor content of cold air. Net radiation is mainly compensated by the subsurface heat flux, which is positive on average (Figure 3f). Since G lags R_{net}, H_S can become significantly negative at daytime (-7 W m^{-2}), which indicates convection. Evidence of convection on the plateau was found by *Mastrantonio et al.* [1999] at Dome C.

[31] The SEB of the four clear-sky days is reproduced well by the model (dotted lines in Figure 3). The larger amplitudes of observed LR fluxes possibly indicate sensor window heating. Another difference between observations and model results is the overestimated modeled sensible heat flux at night. Figure 4 shows average diurnal cycles of the turbulent scales for T, q and U. The overestimated H_S in the model is caused by an overestimation of U_* at night (Figure 4c), which will be discussed in the next section. This does not impact H_L as much because of the very small q_* at night (Figure 4b), as opposed to T_* which does peak at night (Figure 4a). The differences between calculated and modeled T_* and q_* are possibly larger in the first part of the day owing to some icing on the LR_{out} sensor, which is used to determine surface temperature. There is poor agreement between observations and model results for day 30 in Figure 3 due to the presence of clouds and model spin-up.

4.2. Surface Layer

[32] Figure 5 shows the observed and modeled average diurnal cycle of T, q, RH and U at the levels of the PM. The observed daily cycle of T in the SL (Figure 5a) shows stable stratification at night and near-neutral to slightly unstable conditions during the day. Specific humidity follows the same pattern (Figure 5c). Owing to the nonlinear relationship between saturation vapor pressure and temperature a significantly negative gradient in q occurs during the day. RH was similar at all levels; only RH at 2 m is shown (Figure 5e). RH does not show significant stratification so that vertical gradients in q are entirely forced by T. The air is mostly saturated at night. RH values drop to 92% at the end of the convective period.

[33] Wind speed shows a remarkable pattern (Figure 5g). During convection, the wind speed profile is near-logarithmic in shape and the near-surface wind speeds (up to 5 m) attain their maximum values (4 m s^{-1}) around 0900 GMT. Wind speed slowly decreases at all measured levels until a sudden drop occurs at the end of the convective period. In contrast, wind speed at 10 m height peaks during the night (5 m s^{-1}), when a strong stability-related shear in U is present. However, stability decreases from 2200 GMT [*van As et al.*, 2005b] as near-surface wind speed and thus turbulent mixing increases. This causes a decrease in wind shear in the SL during the night. While wind speeds up to 5 m height increase, 10 m wind speed slightly decreases at night.

[34] The model (Figures 5b, 5d, 5f and 5h) simulates the vertical and temporal variations of temperature and humidity in the SL well due to its high near-surface resolution (47 levels in 10 m). The temperature difference between surface and 0.5 m is slightly overestimated and stability at night underestimated (Figure 5b), which is related to the overestimation of U_* in Figure 4c. Also, daytime temperature is slightly too low. Differences in surface temperature can be due to measurement inaccuracy; *van As et al.* [2005a] found that the surface temperatures obtained from LR_{out} measurements are underestimated by 0.8 ± 1.3 K. RH is reproduced very well (Figure 5f). Saturation is modeled during a somewhat longer part of the night than measurements indicate. The simulation of the near-surface wind field is in qualitative agreement with observations (Figure 5h). Nighttime U up to 5 m is too large, which causes the overestimation of U_*. Because of the increased mixing the temperature gradient is underestimated (Figure 5b) and H_S is overestimated (Figure 3d). Clearly, the model does not allow large enough wind speed gradients in stable stratification. Changing the stability-correction function for momentum in stable stratification could provide a solution. However, there is no consensus in literature on which function gives the best results [*Andreas*, 2002], even in the stability regime found during the clear-sky ENABLE days ($z/L_* < 3$ [*van As et al.*, 2005b]). A larger stability correction would improve our model results. In a future

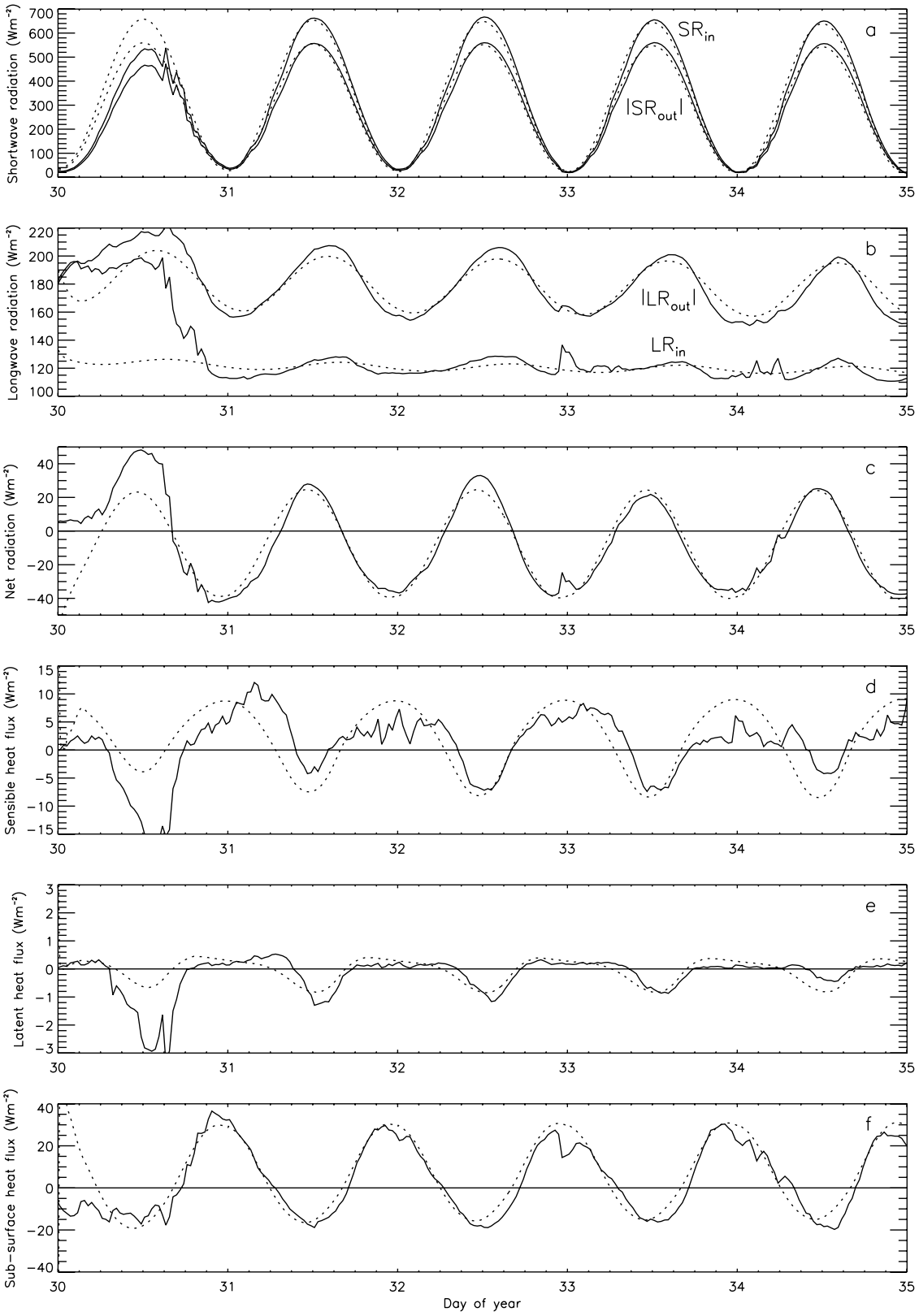

Figure 3. Surface energy balance components between 30 January and 3 February 2002: (a) shortwave radiation, (b) longwave radiation, (c) net radiation, (d) sensible heat flux, (e) latent heat flux and (f) subsurface heat flux, measured/calculated (solid lines) and modeled (dotted lines).

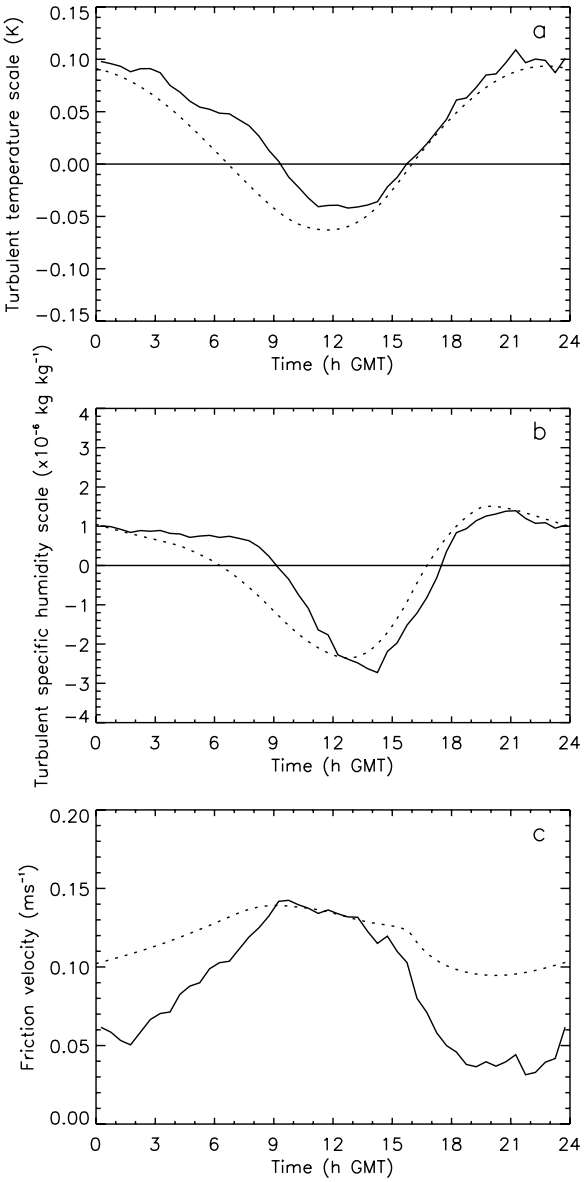

Figure 4. Mean turbulent scales of (a) temperature, (b) moisture, and (c) wind speed, calculated by bulk method (solid lines) and modeled (dotted lines).

study, the profile-mast data will be used to find better suitable stability-correction functions.

4.3. Atmospheric Boundary Layer

[35] Figure 6 presents 4-day mean profiles of θ, q, RH, U and d, measured by tethersonde (solid lines) and radiosonde (dashed lines). Profiles are given for noon (left column) and midnight (right column), since radiosondes were released at these times (∼1100 and 2300 GMT). Ten-meter PM data have been included for reference (triangles).

[36] At noon, a convective layer of near-neutral stability with a depth of 50 m is observed, which is topped by a temperature inversion (Figure 6a). At midnight, a stable layer is present with a temperature deficit of 12 K at the surface (Figure 6b). Above 100 m height, stratification is moderately stable throughout the day. The differences between the observed RS and TS temperature profiles are largely explained by ABL-temperature changes during the 1 hour between the two soundings (Figure 5a).

[37] As in the SL, the q profiles follow temperature (Figures 6c and 6d). Above 100 m altitude q decreases (see also Figure 2b). As discussed in section 3.1, measurements of moisture at low T are less reliable. Inaccuracy increases owing to icing, which especially affects the TS system in the ABL, and response time, possibly affecting the faster-moving RS. Measurement inaccuracy is more apparent for RH (Figures 6e and 6f), which does not indicate saturation in either TS or RS observations, as opposed to the PM observations in Figure 5.

[38] In Figure 6g–6j the mean profiles of wind speed and direction from TS observations are shown. RS U and d measurements are not shown owing to GPS signal loss of the sonde in the lowest few hundred meters. TS wind speed peaks at 70 m height at noon (Figure 6g). A relatively strong wind speed maximum is found at 20 m height at midnight. The nighttime low-level jet is likely to be katabatic in nature as it coincides with the layer of temperature deficit (Figure 6b) over a sloping surface. This is affirmed by the recorded approximate down-slope direction of the near-surface wind in Figure 6j. Wind direction curves to the north with increasing height up to 60 m. At noon the entire convective layer has a uniform direction, above which wind speed is more northerly. We find d at the surface to be approximately down-slope for both midday and midnight (60°), possibly caused by the alignment of the large-scale and katabatic forcings.

[39] In Figure 6 the modeled profiles are presented in dotted lines. The qualitative agreement of simulated θ in the ABL is good. The model produces slightly too low temperatures during the day and too high surface temperatures during the night, as in Figure 5. Modeled T around 100 m height are underestimated by 1–2 K. Owing to measurement inaccuracies the simulated humidity is not easily validated. Again, modeled q follows T. While modeled RH is in good agreement with PM measurements (which are most accurate), TS and RS measurements are clearly lower than the model results. Figures 6e and 6f indicate that the ABL is nearly saturated during the day and is fully saturated up to 40 m height at midnight. Here the model produces clear-sky precipitation. As the modeled RH values below 10 m height are validated by the accurate profile-mast measurements, the modeled RH profiles are more reliable than the TS and RS RH observations in the ABL, which show no saturation at all. Clear-sky precipitation is likely to be overestimated by the model as supersaturation is not allowed in the model, but is known to occur in Antarctica [*King and Anderson*, 1999], and also sublimation of solid precipitation in a layer of unsaturated air is not taken into account.

[40] The wind speed maxima are well reproduced by the model, though ABL wind speeds are 0.5–1 m s^{-1} lower. The simulated wind direction tendency is good; the absolute direction in the ABL is off by 10°–15°. Differences between observed and modeled U and d can be caused by variable geostrophic winds which are assumed constant in the model.

[41] Figure 7 shows the average diurnal cycle of the ABL θ and U as derived from three-hourly TS observations (Figures 7a and 7c) and model results (Figures 7b and 7d).

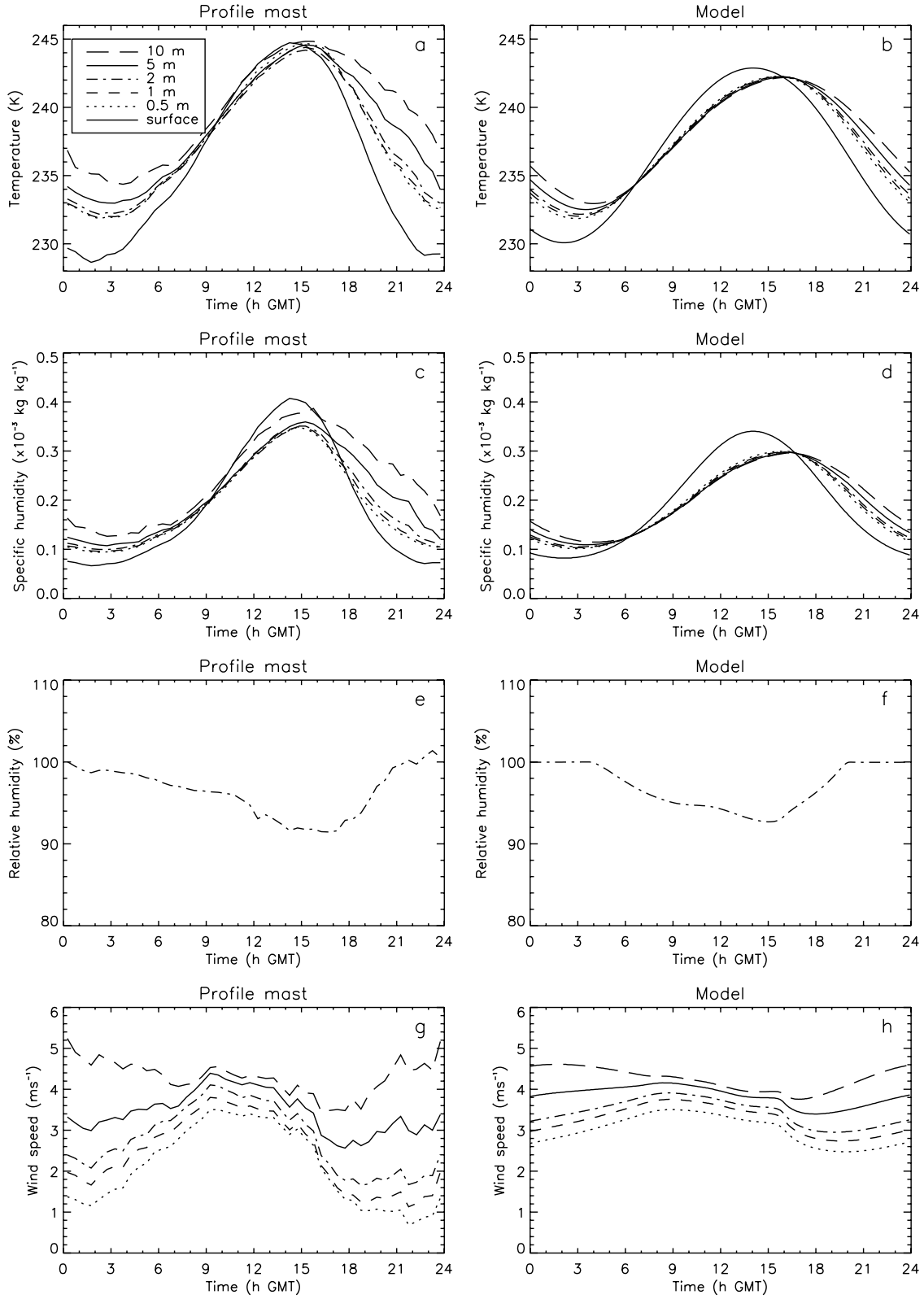

Figure 5. Mean surface layer values of (a, b) temperature, (c, d) specific humidity, (e, f) relative humidity and (g, h) wind speed, measured by profile mast (Figures 5a, 5c, 5e, and 5g) and modeled (Figures 5b, 5d, 5f, and 5h).

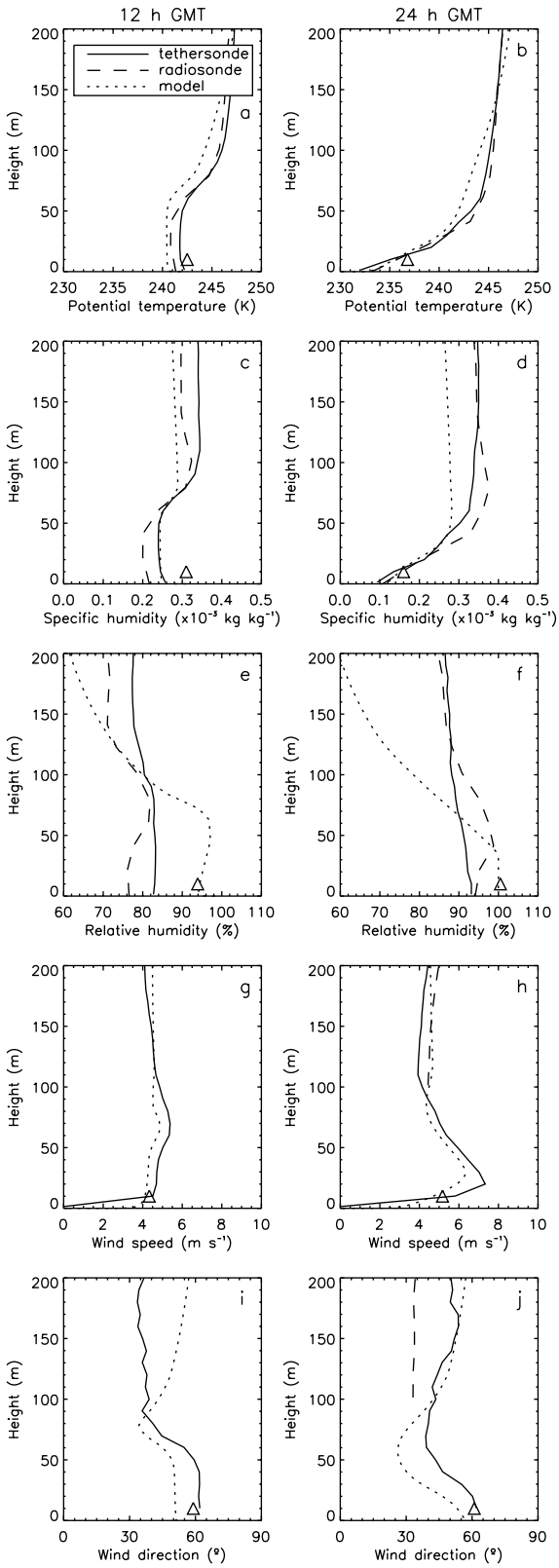

Figure 6. Mean profiles of (a, b) temperature, (c, d) specific humidity, (e, f) relative humidity, (g, h) wind speed, and (i, j) wind direction at ~1200 GMT (Figures 6a, 6c, 6e, 6g, and 6i) and ~2400 GMT (Figures 6b, 6d, 6f, 6h, and 6j), measured by tethersonde (solid lines) and radiosonde (dashed lines) and modeled (dotted lines). Triangles mark 10-m profile mast measurements.

The TS measurements show that the layer of stable stratification grows in thickness during the night. Around 0800 GMT, convection starts at the surface and a mixed layer of near-neutral stability forms which deepens at a rate of 7 m h^{-1}. At the end of the afternoon the convective system collapses and stability increases again during the night. Above the stable layer a residual layer of near-neutral stratification is present.

[42] The increasing thickness of the nighttime stable layer is accompanied by an increasing temperature deficit and increasing speed of the katabatic jet (Figure 7c). The jet persists until convection begins in the morning. However, even after the start of convection, the temperature-deficit layer deepens and stable stratification remains present above the newly formed mixed layer. This causes the katabatic jet to rise. The jet weakens and disappears when convection eliminates the entire temperature-deficit layer. At noon a relatively cold, stably stratified layer is still present at 70 m height, which suggests that the wind maximum in Figure 6g could still be katabatically forced.

[43] The model produces a very similar potential temperature distribution (Figure 7b). Simulated wind speed also shows good qualitative agreement with observations (Figure 7d). The modeled low-level nocturnal jet increases in height during the morning as well. However, we also find a modeled super-geostrophic wind speed in the residual layer in the evening which does not show up so clearly in the observations. The lower part of this layer develops into the nighttime katabatic jet. Between 60 and 100 m height, there is a minimum in U around 0200 GMT and a second maximum forms in the morning hours. The residual layer is possibly subject to an inertial oscillation [*Blackadar*, 1957], which will be discussed in detail by *van As and van den Broeke* [2006].

5. Discussion

[44] The observations of the summertime ABL at Kohnen have shown a very dynamic ABL which is unexpected given the small amount of absorbed shortwave radiation and the small surface slope at Kohnen. Most of the fair-weather ABL dynamics are a result of local forcing and are relatively uninfluenced by large-scale advection. This is supported by the good performance of a 1D high-resolution model in which no horizontal advection terms are included, even though measured free-atmospheric temperatures and winds were not constant.

[45] According to equations (1) and (2) the heat and moisture contents of the ABL can change at the hand of multiple mechanisms. The heat and moisture changes in the daytime convective layer are usually dominated by the turbulent surface fluxes of heat and moisture. The contribution of the turbulent fluxes in the convective ABL can be calculated by dividing the temporally integrated surface flux of a parameter ($\overline{w'a'_0}$) by its total change in the ABL,

$$ratio = \int_{t_1}^{t_2} \overline{w'a'_0}\, dt \Big/ \int_0^{z_{top}} (a_2(z) - a_1(z))\, dz, \qquad (16)$$

where a is here either T or q and subscripts 1 and 2 indicate values at the beginning and end of convection. Using this method we find from the measurements between 0900 and

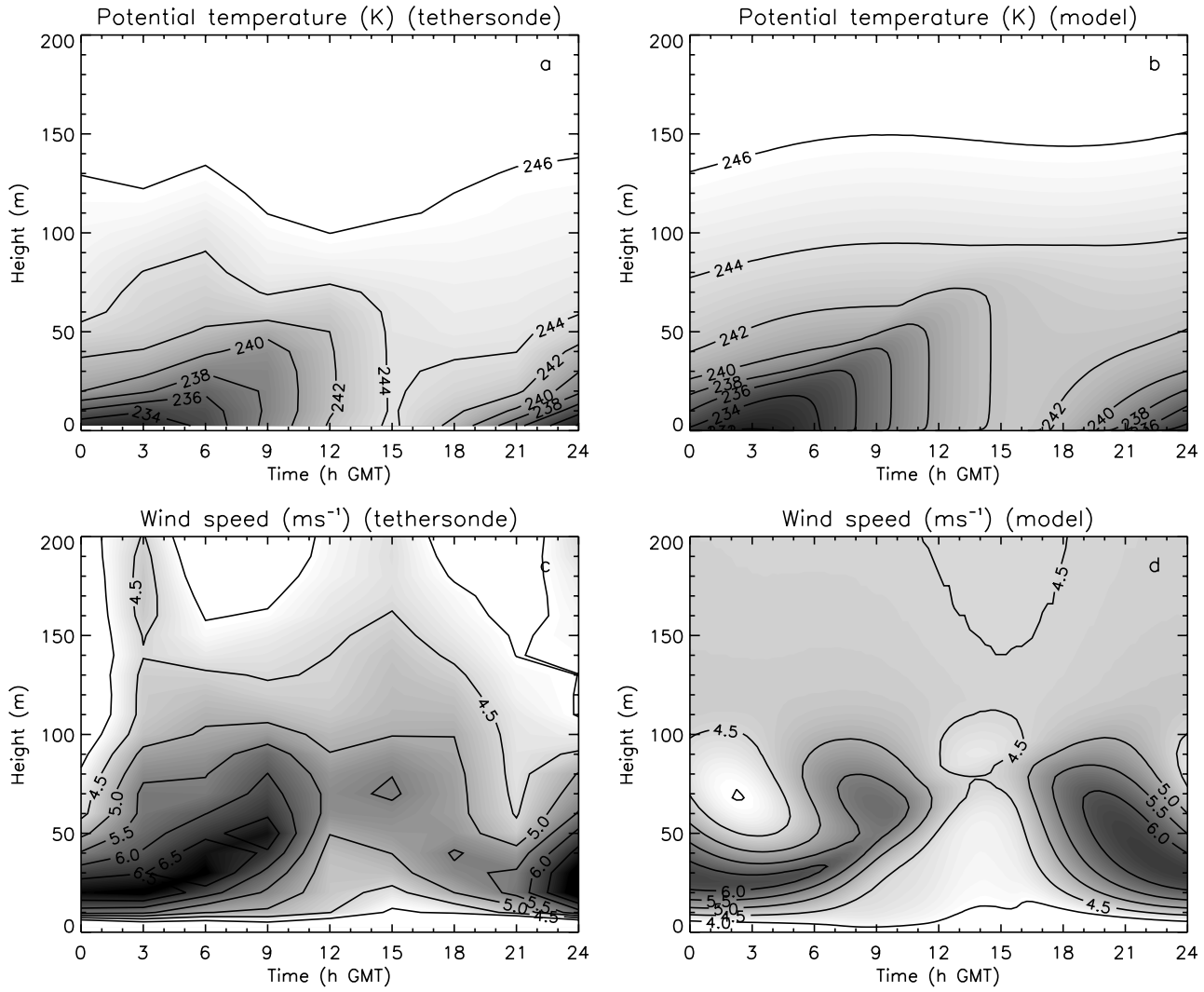

Figure 7. Mean potential (a, b) temperature and (c, d) wind speed, measured by tethersonde (Figures 7a and 7c) and modeled (Figures 7b and 7d).

1500 GMT that the surface turbulent heat flux only provides 28% of the heat necessary to heat the convective layer. For moisture this percentage is higher (59%). The low value for heat suggests that the entrainment flux and/or radiation divergence are relatively large. However, if we perform the same exercise on model results we find that the surface heat flux contributes 64% to convective-layer heating and that virtually all moisture change is caused by the surface moisture flux. The differences between observations and model results originate largely from the differences in measured and modeled T_* and q_* (Figure 4), which are possibly caused by an underestimation of measured surface temperature. The modeled heat and moisture budgets of the summertime ABL at Kohnen are presented by *van As and van den Broeke* [2006].

[46] Figure 8 presents the directional constancy (DC) of the wind, defined as the ratio of the mean to the vector-mean wind speed, as determined from all available 11 days of TS measurements during ENABLE. The figure shows a very persistent wind direction for the nighttime katabatic jet (>0.9). Decreasing DC values with height indicate that the

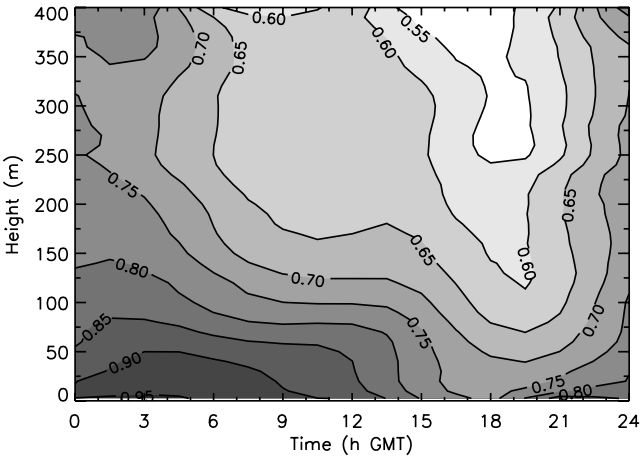

Figure 8. Directional constancy of wind direction over 11 days of tethersonde measurements during ENABLE.

direction of the nocturnal jet is determined at the surface and that wind direction is increasingly more influenced by the variable geostrophic winds for larger altitude. The figure also shows a dip in DC values in the ABL between 1500 and 2400 GMT which can either be the result of an increase in free-atmospheric influence when the residual layer becomes frictionally decoupled from the surface or the simultaneously observed dip in free-atmospheric DC. Free-atmospheric DC values are fairly high (0.5–0.8), but vary during the day. TS observations over a longer period would result in a more constant DC for the large-scale winds.

[47] Using ENABLE radiosonde observations covering the period from 9 January to 10 February 2002 we find the following mean geostrophic wind components:

$$u_g = -2.3 + 0.95 \times 10^{-3} z$$

$$v_g = -5.9 + 1.29 \times 10^{-3} z,$$

where u and v are now oriented in zonal and meridional direction, respectively. Extrapolation downwards of these profiles shows that the geostrophic wind direction at the surface is 21°, which is close to the upward surface slope direction of 61°. Since the wind direction of the convective ABL is determined by the geostrophic wind direction and possibly katabatic forcing, the nighttime stable layer and daytime mixed layer are thus forced in the approximate same direction, which is the cause of the small cycle in wind direction in the summertime surface layer at Kohnen [*van As et al.*, 2005b].

[48] The vertical shear in the geostrophic wind is related to a mesoscale horizontal temperature gradient which is described by the thermal wind balance,

$$\frac{\partial u_g}{\partial z} = -\frac{g}{fT}\frac{\partial T}{\partial y} \qquad \frac{\partial v_g}{\partial z} = \frac{g}{fT}\frac{\partial T}{\partial x}. \tag{17}$$

The measured geostrophic wind shear translates into a horizontal T gradient of 0.56 K per 100 km toward 306°, which is perpendicular to the South Atlantic coast line in this part of DML. This agrees with the mean temperature field for January 2002 as derived from ERA-40 data, which slopes toward 301°, though with a smaller gradient (0.35 K per 100 km). *Bintanja* [2000] found mesoscale horizontal temperature gradients of at most 0.6 K per 100 km for the Svea area (Figure 1) in the austral summer of 1997/1998. *Kodama et al.* [1989] used a similar approach as presented above to calculate the summertime mesoscale horizontal temperature gradient for Adélie Land, Antarctica, and found the much larger gradient of 2.5 K per 100 km. The smaller contrast in free-atmospheric temperatures in the DML area is possibly caused by a more southerly location and the relatively cold air over the ice-covered Weddell Sea.

6. Summary

[49] In this paper we presented profile-mast, tethersonde and radiosonde observations of the clear-sky atmospheric boundary layer for a period at the end of summer at Kohnen base, which is situated on the Antarctic Plateau. Daily mean net radiation was small and negative. The latent heat flux was very small (<1 W m^{-2}) owing to the low moisture content of air at low temperatures. The sensible heat flux contributed less than 10 W m^{-2} to the surface energy budget.

[50] In spite of the weak energy exchange found at the snow surface, a dynamic atmospheric boundary layer was observed. Convection caused the formation of a shallow mixed layer (maximum 70 m deep) during the day. Surface fluxes of heat and moisture accounted for 28 and 59% of the change in boundary-layer heat and moisture content during convection, respectively. Relative humidity near the surface reached a minimum value of 92% around 1500 GMT. In the evening the atmosphere started cooling near the surface, creating an increasingly deep stable and saturated layer. No fog was observed during this clear-sky period; saturation presumably leads to the formation of solid precipitation (diamond dust). The nighttime stable layer obtained a maximum temperature deficit of 12 K, which resulted in a katabatically driven nocturnal jet with a strength of 7.4 m s^{-1} at midnight. This layer reached a thickness of 50 m in the morning, but even continued to grow after convection had started at the surface. A wind maximum was still measured at 70 m altitude around noon.

[51] Radiosonde observations indicated that the geostrophic wind direction is approximately equal to the surface slope direction, which explains the small daily cycle in wind direction in the atmospheric boundary layer at Kohnen. The shear of the wind profile is the result of a mesoscale horizontal temperature gradient of 0.56 K per 100 km, which is due to the free-atmospheric temperature difference between the air over the South Atlantic Ocean and the Antarctic interior.

[52] A high-resolution one-dimensional model was used to simulate the atmospheric boundary layer for the same fair-weather period. The qualitative agreement of the boundary layer structure and dynamics between observations and simulation was very good. Surface layer temperatures were slightly underestimated during the day. An overestimation of nighttime friction velocity resulted in too much vertical mixing and therefore an underestimation of stability and a less pronounced katabatic wind maximum. Model results indicate that wind maxima in the atmospheric boundary layer at Kohnen base can possibly be partly explained by the occurrence of inertial oscillations. The dynamics of the modeled clear-sky atmospheric boundary layer are discussed in the context of its heat, moisture and momentum budgets in a companion paper [*van As and van den Broeke*, 2006].

[53] **Acknowledgments.** We thank the Alfred-Wegener-Institute (AWI) for providing logistics for the ENABLE expedition and the Netherlands Polar Programme (NPP) for financial support. This work is a contribution to the "European Project for Ice Coring in Antarctica" (EPICA), a joint ESF (European Science Foundation)/EC scientific program, funded by the European Commission and by national contributions from Belgium, Denmark, France, Germany, Italy, Netherlands, Norway, Sweden, Switzerland and the United Kingdom. This is EPICA publication 149.

References

Anderson, P. S. (1994), A method for rescaling humidity sensors at temperatures well below freezing, *J. Atmos. Oceanic Technol.*, *11*, 1388–1391.

Anderson, P. S. (1996), Reply to "Comments on 'A method for rescaling humidity sensors at temperatures well below freezing,'" *J. Atmos. Oceanic Technol.*, *13*, 913–914.

Andreas, E. L. (1987), A theory for the scalar roughness and the scalar transfer coefficients over snow and sea ice, *Boundary Layer Meteorol.*, *38*, 159–184.

Andreas, E. L. (2002), Parameterizing scalar transfer over snow and ice: A review, *J. Hydrometeorol.*, *3*, 417–432.

Ball, F. K. (1956), The theory of strong katabatic winds, *Aust. J. Phys.*, *9*, 373–386.

Bintanja, R. (2000), Mesoscale meteorological conditions in Dronning Maud Land, Antarctica, during summer: A qualitative analysis of forcing mechanisms, *J. Appl. Meteorol.*, *39*, 2348–2370.

Blackadar, A. K. (1957), Boundary layer wind maxima and their significance for the growth of nocturnal inversions, *Bull. Am. Meteorol. Soc.*, *38*(5), 283–290.

Brost, R. A., and J. C. Wyngaard (1978), A model study of the stably stratified planetary boundary layer, *J. Atmos. Sci.*, *35*, 1427–1440.

Curry, J. A., and P. J. Webster (1999), *Thermodynamics of Atmospheres and Oceans*, Elsevier, New York.

Deardorff, J. W. (1978), Efficient prediction of ground surface temperature and moisture, with inclusion of a layer of vegetation, *J. Geophys. Res.*, *83*(C4), 1889–1903.

Duynkerke, P. G. (1991), Radiation fog—A comparison of model simulation with detailed observations, *Mon. Weather Rev.*, *119*(2), 324–341.

Dyer, A. J. (1974), A review of flux-profile relationships, *Boundary Layer Meteorol.*, *7*, 363–372.

Fouquart, Y., and B. Bonnel (1980), Computations of solar heating of the Earth's atmosphere: A new parameterization, *Beitr. Phys. Atmos.*, *53*, 35–62.

Heinemann, G. (1988), On the structure and energy budget of the boundary layer in the vicinity of the Filchner/Ronne ice shelf front (Antarctica), *Beitr. Phys. Atmos.*, *61*, 244–258.

Holtslag, A. A. M., and H. A. R. de Bruin (1988), Applied modelling of the night-time surface energy balance over land, *J. Appl. Meteorol.*, *27*, 689–704.

King, J. C. (1989), Low-level wind profiles at an Antarctic coastal station, *Antarct. Sci.*, *1*(2), 169–178.

King, J. C., and P. S. Anderson (1999), A humidity climatology for Halley, Antarctica, based on frost-point hygrometer measurements, *Antarct. Sci.*, *11*(1), 100–104.

Kodama, Y., G. Wendler, and N. Ishikawa (1989), The diurnal variation of the boundary layer in summer in Adélie Land, eastern Antarctica, *J. Appl. Meteorol.*, *28*, 16–24.

Kottmeier, C. (1986), Shallow gravity flows over the Ekström ice shelf, *Boundary Layer Meteorol.*, *35*, 1–20.

Liu, H., K. Jezek, B. Li, and Z. Zhao (2001), Radarsat Antarctic Mapping Project digital elevation model version 2, http://nsidc.org/data/nsidc-0082.html, Natl. Snow and Ice Data Cent., Boulder, Colo.

Mahesh, A., V. P. Walden, and S. G. Warren (1997), Radiosonde measurements in strong inversions: Correction for thermal lag based on an experiment at the South Pole, *J. Atmos. Oceanic Technol.*, *14*, 45–53.

Mastrantonio, G., V. Malvestuto, S. Argentini, T. Georgiadis, and A. Viola (1999), Evidence of a convective boundary layer developing on the Antarctic Plateau during the summer, *Meteorol. Atmos. Phys.*, *71*(1–2), 127–132.

Nieuwstadt, F. T. M. (1984), The turbulent structure of the stable, nocturnal boundary layer, *J. Atmos. Sci.*, *41*, 2202–2216.

Östin, R., and S. Andersson (1991), Frost growth-parameters in a forced air stream, *Int. J. Heat Mass Transfer*, *34*(4–5), 1009–1017.

Parish, T. R., and J. J. Cassano (2003), Diagnosis of the katabatic wind influence on the wintertime Antarctic surface wind field from numerical simulations, *Mon. Weather Rev.*, *131*(6), 1128–1139.

Renfrew, I. A. (2004), The dynamics of idealized katabatic flow over a moderate slope and ice shelf, *Q. J. R. Meteorol. Soc.*, *130*(598), 1023–1045.

Rodgers, C. D. (1967), The radiative heat budget of the troposphere and lower stratosphere, *Rep. N012 A2*, Planet. Circ. Proj., Dep. of Meteorol, Mass. Inst. of Technol., Cambridge, Mass.

Sorbjan, Z., Y. Kodama, and G. Wendler (1986), Observational study of the atmospheric boundary layer over Antarctica, *J. Clim. Appl. Meteorol.*, *25*, 641–651.

van As, D., and M. R. van den Broeke (2006), Structure and dynamics of the summertime atmospheric boundary layer over the Antarctic Plateau: 2. Heat, moisture, and momentum budgets, *J. Geophys. Res.*, *111*, D07103, doi:10.1029/2005JD006956.

van As, D., M. R. van den Broeke, C. H. Reijmer, and R. S. W. van de Wal (2005a), The summer surface energy balance on the high Antarctic Plateau, *Boundary Layer Meteorol.*, *115*, 289–317, doi:10.1007/s10546-004-4631-1.

van As, D., M. R. van den Broeke, and R. S. W. van de Wal (2005b), Daily cycle of the surface layer and energy balance on the high Antarctic Plateau, *Antarct. Sci.*, *17*(1), 121–133.

van den Broeke, M. R., N. P. M. van Lipzig, and E. van Meijgaard (2002), Momentum budget of the East Antarctic atmospheric boundary layer: Results of a regional climate model, *J. Atmos. Sci.*, *59*, 3117–3129.

van den Broeke, M. R., D. van As, C. H. Reijmer, and R. S. W. van de Wal (2004), Assessing and improving the quality of unattended radiation observations in Antarctica, *J. Atmos. Oceanic Technol.*, *21*, 1417–1431.

M. M. Helsen, D. van As, and M. R. van den Broeke, Institute for Marine and Atmospheric Research Utrecht (IMAU), Utrecht University, PO Box 80000, 3508 TA, Utrecht, Netherlands. (d.vanas@phys.uu.nl)